

A Review of Deep Learning CT Reconstruction From Incomplete Projection Data

Tao Wang^{ID}, *Student Member, IEEE*, Wenjun Xia^{ID}, *Member, IEEE*, Jingfeng Lu, and Yi Zhang^{ID}, *Senior Member, IEEE*

Abstract—Computed tomography (CT) is a widely used imaging technique in both medical and industrial applications. However, accurate CT reconstruction requires complete projection data, while incomplete data can result in significant artifacts in the reconstructed images, compromising their reliability for subsequent detection and diagnosis. As a result, accurate CT reconstruction from incomplete projection data remains a challenging research area in radiology. With the rapid development of deep learning (DL) techniques, many DL-based methods have been proposed for CT reconstruction from incomplete projection data. However, there are limited comprehensive surveys that summarize recent advances in this field. This article provides a comprehensive overview of the current state-of-the-art DL-based CT reconstruction from incomplete projection data, including sparse view reconstruction, limited angle reconstruction, metal artifact reduction, interior tomography, and ring artifact reduction. This survey covers various DL-based solutions to the five problems, potential limitations of existing methods, and future research directions.

Index Terms—Computed tomography (CT), deep learning (DL), interior tomography (IT), limited angle (LA), metal artifact reduction (MAR), ring artifact reduction, sparse view (SV).

I. INTRODUCTION

COMPUTED tomography (CT) is an imaging technique that generates cross-sectional data of an object by gathering ray projections from various angles. It is a noninvasive and nondestructive approach that can efficiently reconstruct high-resolution images of objects' internal structures. The resulting images provide excellent contrast, enabling differentiation between tissues, organs, and lesions, thus facilitating

Manuscript received 24 June 2023; revised 19 August 2023; accepted 7 September 2023. Date of publication 15 September 2023; date of current version 5 February 2024. This work was supported in part by the National Natural Science Foundation of China under Grant 62271335; in part by the Sichuan Science and Technology Program under Grant 2021JDJQ0024; and in part by the Sichuan University "From 0 to 1" Innovative Research Program under Grant 2022SCUH0016. (*Corresponding author: Yi Zhang*)

This work involved human subjects or animals in its research. The authors confirm that all human/animal subject research procedures and protocols are exempt from review board approval.

Tao Wang and Wenjun Xia are with the College of Computer Science, Sichuan University, Chengdu 610065, China, and also with the Key Laboratory of Data Protection and Intelligent Management, Ministry of Education, Sichuan University, Chengdu 610207, China.

Jingfeng Lu is with the School of Cyber Science and Engineering, Sichuan University, Chengdu 610065, China.

Yi Zhang is with the School of Cyber Science and Engineering, Sichuan University, Chengdu 610065, China, and also with the Key Laboratory of Data Protection and Intelligent Management, Ministry of Education, Sichuan University, Chengdu 610207, China (e-mail: yzhang@scu.edu.cn).

Color versions of one or more figures in this article are available at <https://doi.org/10.1109/TRPMS.2023.3316349>.

Digital Object Identifier 10.1109/TRPMS.2023.3316349

accurate diagnoses. CT has emerged as a critical diagnostic tool and has revolutionized the field of medicine.

The quality of the reconstructed images from CT scans is directly influenced by the completeness of the measured data. Accurate CT images can be reconstructed from complete projection data using classic analytical or iterative reconstruction methods, resulting in high-quality images. However, complete projection data may not be available in practice, due to factors, such as radiation dose limitations, space and time constraints, object shape, and imaging system limitations. Owing to the incompleteness of the projection data, artifacts significantly impact the quality of the reconstructed CT images. As a result, incomplete projection data reconstruction has become a hot research topic with significant practical value.

Before deep learning (DL) is widely used, early methods for incomplete projection data reconstruction can be divided into two categories: 1) projection data completion methods and 2) iterative reconstruction methods. The former methods start from the projection data and use the known information to estimate the missing projection data [1], [2], [3], [4], [5], [6], [7], [8]. Iterative reconstruction formulates an objective function based on the observation and prior knowledge of CT images, subsequently attaining the solution through the optimization of this function. This process begins with an initial image estimation and gradually improves the quality of this estimation under the guidance of measured projection data and prior knowledge. From a Bayesian theory perspective, the model of iterative reconstruction can be characterized as a Maximum a Posteriori model [9]

$$\log p(\boldsymbol{\mu}|\mathbf{y}) \propto \log p(\mathbf{y}|\boldsymbol{\mu}) + \log p(\boldsymbol{\mu}) \quad (1)$$

where $\boldsymbol{\mu}$ denotes the image to be reconstructed, and \mathbf{y} is the measured projection data. $\log p(\mathbf{y}|\boldsymbol{\mu})$ represents the log-likelihood, which is developed using a fidelity term. $\log p(\boldsymbol{\mu})$ symbolizes the logarithm of the prior probability, built using a regularization term. Typical prior-based regularization terms include total variation [10], dictionary learning [11], and low-rank [12], to name a few. Although these methods are effective, they come with a significant computational cost. Moreover, the regularization models require fine-tuning with careful adjustment of hyperparameters; otherwise, inappropriate parameters can lead to reconstruction deviation. This is especially problematic for highly incomplete projection data reconstruction and poses challenges to the clinical application of iterative algorithms.

In recent years, DL shows great potential in medical image processing [13], [14], [15], [16], [17], [18], [19], [20], [21].

A wide variety of DL-based methods have emerged and brought new solutions to incomplete projection data reconstruction [22], [23], [24], [25], [26], [27], [28], [29]. However, to the best of our knowledge, there are limited comprehensive reviews that discuss and summarize the application of DL in incomplete projection data reconstruction. In this article, we conduct a comprehensive investigation of existing DL-based methods for incomplete projection data reconstruction, including sparse view (SV) CT reconstruction, limited angle (LA) CT reconstruction, metal artifact reduction (MAR), and interior tomography (IT) and ring artifact reduction.

The rest of this article is organized as follows. Section II introduces the causes of incomplete projection data. Section III reviews the main contents of recent DL-based methods for CT reconstruction from incomplete projection data. Evaluations are presented in Section IV. Section V concludes this article, lists limitations, and presents potential directions that are worthy of further investigation.

II. CAUSES OF INCOMPLETE PROJECTION DATA

This article focuses on CT reconstruction from incomplete projection data, including incomplete sampling view problems, metal implant problems, and interior problems, which have received much attention recently. Fig. 1 depicts both complete and incomplete projection data reconstructions.

In parallel-beam imaging systems, when the scanning angle is 360° , it is a full scan, and 180° is called a half scan, which is the minimum angle range required for accurate reconstruction. In fan-beam imaging systems, the quality of the reconstructed image is related to the scanning range. In the fan-beam situation, the half-scanning range is $180 + \omega^\circ$, where the ω is the field angle of the fan beam. This survey takes the fan-beam scanning system as an example, since fan-beam is more realistic and more commonly studied. As recent works [30], [31], we take the full scan to obtain complete projection data.

A. Incomplete Sampling View Problem

The incomplete sampling view problems specifically correspond to two situations, including SV sampling problem and LA sampling problem, where only part of the projection data within the full scan range is obtained.

SV sampling is usually used to reduce radiation exposure to the human body. In addition, it can shorten scanning time and reduce motion artifacts due to shaking, heart beating, and respiratory motion. Due to the missing projection data at some angles, streak artifacts are introduced into the reconstructed image, where important details may be impaired.

LA scanning is applied in when the scanning region or system hardware is limited and the radiation source can only rotate within a limited angle range. For example, due to the limitation of imaging object structure, and system scanning geometric position, the acquired data miss some projections in a continuous angle range, resulting in LA sampling. In the case of LA sampling, the reconstructed CT images usually suffer from directional artifacts and structural distortions.

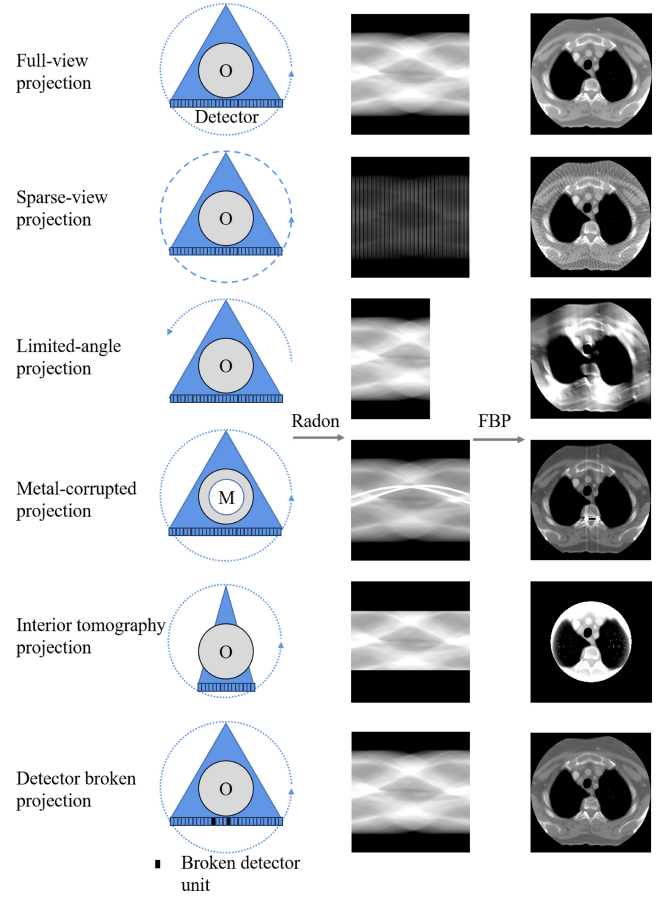


Fig. 1. Comprehensive illustration of full and incomplete projection data reconstructions in fan-beam geometry. Here, “O” represents the object, and “M” stands for the metal. The blue dotted line indicates the X-ray scanning trajectory, with the blue triangle signifying the field of view of a single projection.

B. Metal Implant Problem

For scanning regions that contain metal objects, the X-ray will undergo severe attenuation. For example, CT scanning regions often encounter substances with high-attenuation coefficients, such as metal implants, fracture intramedullary nails, steel plates, cardiac pacemakers, vascular stents, artificial hip joints, and metal dentures. Metal implant problem is a typical external problem in practical applications. As X-rays pass through metals, most of the photons are absorbed, leading to challenges to detect tissue information on these X-rays. This results in incomplete projection data, with important information missing. There will be alternating light and dark artifacts in the reconstructed image, known as metal artifacts. These metal artifacts obstruct and disrupt the identification of organs and lesions, thereby impacting subsequent analysis and diagnosis.

C. Interior Problem

In the interior reconstruction problem, the field of projection view ray cannot cover the entire space of the scanned object, and only the projection data for the internal region of interest (ROI) are collected. It is a typical data truncation problem and belongs to the case of local reconstruction, which

TABLE I
REPRESENTATIVE DL-BASED METHODS FOR CT RECONSTRUCTION FROM INCOMPLETE PROJECTION DATA

References	Problems	Datasets	Highlights
Dong et al. [22]	SV	Non-public	U-Net and residual learning to complete sinogram
Lee et al. [23]	SV	Non-public	replacing pooling with strided convolution
Okamoto et al. [39]	SV	Chest dataset [93]	band patch-based, light-weight network
Xie et al. [54]	SV	Non-public	GoogLeNet and residual learning
Zhang et al. [55]	SV	NBIA	DenseNet and deconvolution
Jin et al. [25]	SV	AAPM	multi-resolution decomposition
Han et al. [56]	SV	AAPM	meet the frame condition, multi-resolution
Zhou et al. [30]	SV, MAR	Deeplesion	recurrent dual-domain, data consistent layer
Wu et al. [94]	SV	NBIA	deep priors with CS iterative reconstruction
Li et al. [75]	SV	Non-public	for a variety of reconstruction problems
He et al. [76]	SV	Mayo Clinic	inverse Radon transform approximation
Kandarpa et al. [78]	SV	Lung-PET-CT-Dx [95]	FBP downsmiling concatenations, domain transformation
Anirudh et al. [41]	LA	Luggage CT	a system of 1D and 2D convolutional neural networks
Huang et al. [51]	LA	AAPM	integrating the data consistency and the prior information
Zhou et al. [79]	LA	DeepLesion	unsupervised sinogram adaptation
Hu et al. [70]	LA	AAPM	single-shot projection error correction, progressive-improvement strategy
Zhou et al. [31]	SV, LA	Deeplesion	cascaded residual dense spatial channel attention, projection data fidelity layer
Chen et al. [71]	LA	AAPM	multi-stage self-constraints, cross-domain optimization, self-augmented learning
Liao et al. [80]	MAR	DeepLesion, Spineweb	disentangling metal-affected images into different domains without paired data
Lee et al. [86]	MAR	DeepLesion, Spineweb	introducing a disentanglement parameter
Niu et al. [82]	MAR	DeepLesion, Spineweb	low-dimensional patch manifold representation
Lin et al. [29]	MAR	DeepLesion	dual domain, Radon inversion layer, Radon consistency loss
Lin et al. [67]	MAR	DeepLesion	encoding mask projection for sinogram restoration, metal-affected data as input
Lyu et al. [60]	MAR	DeepLesion	deep prior image network for sinogram prior
Wang et al. [72]	MAR	DeepLesion	adaptive scaling, residual learning, long-range dependencies of metal artifacts
Wang et al. [68]	MAR	DeepLesion	hybrid prior estimations, parallel interactive branches on dual domain
Lyu et al. [83]	MAR	DeepLesion	unpaired dual-domain network exploiting the additive artifacts property
Han et al. [52]	IT	AAPM	removing null space signals
Han et al. [53]	IT	AAPM	taking the truncated differentiated back projection data as input
Han et al. [64]	IT	AAPM	solve a coupled low-dose interior problem
Chen et al. [65]	IT	AAPM	extraction-based dual-domain network
Nauwynck et al. [96]	Ring artifact	Cancer Imaging Archive [95]	normalized loss function operating on sinogram
Chang et al. [33]	Ring artifact	AAPM	generate a hybrid corrected image with network output and pre-corrected image
Liu et al. [34]	Ring artifact	AAPM	achieve noise reduction and ring artifact removal simultaneously
Fu et al. [97]	Ring artifact	AAPM	CNN detects the stripes and RNN processes the line artifact correction

is commonly used in dental imaging where the focus is on the teeth rather than the entire head region. The interior imaging method can greatly reduce the X-ray radiation received by the external area of ROI and reduce the size of the detector, leading to cost-effective imaging systems and solving the imaging problem of large objects. To this end, accurate reconstruction from truncated projection data is of great significance.

D. Ring Artifact Problem

Ring artifact is a common type of artifact in CT imaging, which mainly originates from the suboptimal performance of the flat-panel detector. This can be attributed to several factors, including the nonuniform response of detector elements, and changes in temperature or beam strength [32], [33], [34]. These artifacts appear as lines along the detector dimension in the sinogram domain. Within the image domain, they occur in the form of concentric circles, with their center positioned around the reconstruction point. These circles display alternating brightness patterns, varying in width from wide to narrow. The existence of ring artifacts compromises the quality of CT images, thus affecting subsequent image processing and clinical diagnosis. It is necessary to mitigate these artifacts.

CT reconstruction obtains images from the observed projection data, which is essentially an inverse problem. When the projection data is incomplete, only a small number of pixels contribute to a nonzero attenuation value, and the corresponding system matrix has sparsity. In addition, due to X-ray beam

hardening, scattering, photon statistics, and detector inaccuracy, noise can also be easily introduced, leading to inaccurate solutions. If effective solutions are not adopted, reconstructed CT images are inapplicable to clinical scenarios. This article focuses on incomplete projection data reconstruction problems and the DL-based solutions to these problems. It is desired to bring new inspiration to address these problems.

III. REVIEW OF CURRENT DEEP-LEARNING-BASED METHODS

In recent times, there has been a widespread interest in DL technology. Several DL-based approaches have been introduced and have yielded impressive results. In this section, we explore how these methods have utilized DL technology to reconstruct CT images from incomplete projection data. Table I summarizes representative DL-based methods.

A. Different Domain Learning

DL-based methods can be classified into four distinct groups based on the data domains they operate. These categories include sinogram domain learning, image domain learning, dual-domain learning, and domain transformation learning. Fig. 2 depicts the classification of different domain learning methods for incomplete projection data reconstruction.

1) *Sinogram Domain Learning*: A common incomplete projection data reconstruction approach is to directly fill in the

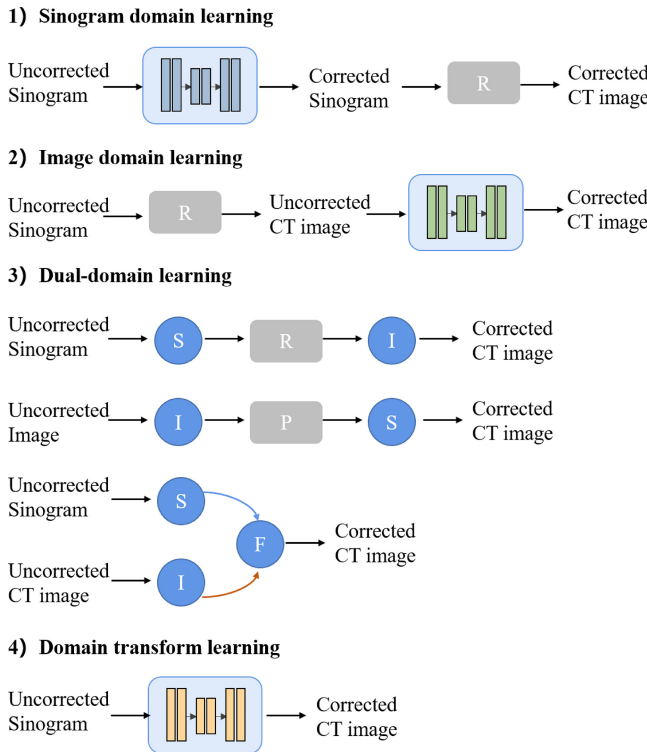


Fig. 2. Classification of DL-based incomplete projection data reconstruction methods. S: Sinogram domain network. I: Image domain network. P: Projection operation. R: Reconstruction operation. F: Dual-domain information fusion operation.

missing data or replace corrupted data, which is akin to interpolation in the case of SV, LA, and MAR, or extrapolation for IT. After the projection data has been corrected, traditional CT reconstruction techniques like filtered back projection (FBP) can be used to obtain the final CT images.

As an instance, Dong et al. [22] combined U-Net [35] to obtain a complete sinogram and preliminarily demonstrated that DL is an effective solution to inpaint the sinogram. Due to the benefits of residual learning [36], such as facilitating training and improving gradient flow, it has been widely employed. Lee et al. [23] modified the U-Net architecture by substituting pooling layers with strided convolution layers to prevent information loss. Li et al. [37] proposed to consider the sequence features of projection data at adjacent angles by incorporating long short-term memory network (LSTM) [38] into the residual U-Net. To enhance the efficiency in clinical settings, Okamoto et al. [39] proposed a band patch-based lightweight fully convolutional network for sinogram inpainting and achieved a fivefold speedup compared to the U-Net-based methods. Additionally, to generate more realistic sinograms, several studies integrated adversarial learning techniques into training process [40], [41].

Projection domain MAR methods can be classified into two types, considering whether they utilize the projection data in the metal region. The first type is the sinogram enhancement method, which is under the assumption that the projection data in the metal region contains valuable information. The effectiveness of such methods is affected by the energy and intensity of the X-ray source emitting photons. If the X-ray

source fails to emit photons with sufficient energy and intensity to penetrate metal objects, the correction of metal artifacts may not be feasible because valid radiation attenuation information from the projected data in the metal region is unavailable. On this basis, Ghani and Karl [24] and Park et al. [42] employed convolutional neural networks to enhance the projection data. The corrected sinogram closely resembled the target sinograms, demonstrating the effectiveness of these methods in restoring accurate projection values.

The second one is the sinogram completion method, which assumes that the projection data in the metal region is completely missing or severely degraded due to photon starvation or scatter, to name a few. Similar to traditional projection domain data completion methods [43], [44], the missing or degraded data in the metal region are estimated by leveraging information from adjacent regions that are not affected by metal artifacts. For example, Pimkin et al. [45] and Peng et al. [46] utilized partial convolution [47] to gradually fill in the contaminated projection data using only the projection data outside the metal trace, which was considered as clean data.

Li et al. [48] conducted a comparative study between sinogram enhancement and sinogram completion methods and discovered that sinogram enhancement was more efficient in MAR. However, they observed that sinogram enhancement requires precise metal masks for a stable performance. If the metal masks are not accurately recognized, the results from the sinogram enhancement method may be imprecise or unreliable.

It is noteworthy that every value in the projection data is associated with all pixels on a ray path in the image domain, making each projection data more informative. Thus, even small inaccuracies in the projection domain can spread over the entire image domain via the back projection process, thus resulting in secondary artifacts. Particularly, when there is a significant amount of missing projection data, it is challenging to achieve accurate estimations. In addition, maintaining the boundary consistency of the metal trace is important yet challenging in both sinogram enhancement and sinogram completion methods.

2) Image Domain Learning: Image-domain learning is a post-processing approach, that trains neural networks to map an input CT image affected by noise and artifacts to a clean CT image.

Zhang et al. [49], Huang et al. [50], [51], and Han et al. [52], [53] proposed end-to-end DL-based approaches to learn the mapping from FBP results to artifact-free images for CT artifacts reduction. Despite using a simple forward neural network architecture, their methods demonstrated superior performance compared to traditional and DL-based projection domain methods. Similar to sinogram domain methods, residual learning has been incorporated into DL-based image domain methods for artifact reduction. For example, Xie et al. [54] combined residual learning with the GoogLeNet for streak artifact reduction. Zhang et al. [55] incorporated residual learning into the DenseNet and combined it with deconvolution to further enhance the feature representation ability of the U-Net. Jin et al. [25] proposed FBPCoVNet that integrated FBP, U-Net, and residual learning.

U-Net has become a popular choice for CT image artifact reduction. Nonetheless, according to Han and Ye [56], U-Net is theoretically proven not to meet the frame condition [57]. Moreover, they found that U-Net tends to overly focus on the low-frequency component of the input image, resulting in blurred artifacts in the corrected images. To address this issue, they introduced a dual-frame U-Net that satisfies the frame condition. Furthermore, they proposed a tight frame U-Net, which integrated wavelet decomposition into the sub band signal processing to achieve better-artifact reduction performance.

In MAR, Zhang and Yu [58] proposed a DL-based framework, which is an open framework that can incorporate the results of different MAR methods to enhance the performance. To further improve the artifact reduction performance, Gjestebry et al. [59] incorporated detailed images derived from filtering as an auxiliary input. Although efforts have been made to correct images, the absence of original projection data could result in suboptimal preservation of anatomical structure details [60]. Obtaining complete projection data is the foundation for the accurate reconstruction of FBP. However, under incomplete projection data conditions, FBP will generate images with significant artifacts. In the DL-based image domain methods, if these FBP results are taken as inputs, corrected results by networks will also be influenced. Taking MAR as an example, the input image is generally an uncorrected image or a linear interpolation-corrected image. In the former case, artifacts are retained after correction. In the latter case, the corrected image contains fewer artifacts while losing tissue details near the metal due to linear interpolation correction.

3) Dual-Domain Learning: Although the above DL-based sinogram and image domain algorithms have significantly improved the artifact reduction performance compared with traditional methods, these single-domain methods still have some limitations. Secondary artifacts are easily introduced in sinogram domain DL-based methods. While in image domain DL-based methods, recovering information that has been lost from raw data can be a challenging task. To effectively extract information from both sinogram and image domains and complement each other, dual-domain networks have been integrated in this learning manner.

Liang et al. [61] and Zhang et al. [28] connected the sinogram and image domain networks with a differentiable reconstruction layer. The constraints were imposed in both sinogram and image domains simultaneously. The projection data could also be corrected by the error information propagating back from the image domain, thus suppressing the secondary artifacts. Zhou et al. [30] proposed to construct an artifact-free image by recurrent image domain and sinogram domain networks. However, the proposed method requires high-computing resources. When deploying the models in practice, the models should be lightweight and efficient. Sun et al. [62] introduced shuffle blocks of ShuffleNet V2 [63] to reduce the number of parameters without performance loss. Hybrid loss functions (structural similarity loss, adversarial loss, and total variation loss) were employed in the dual domains to ensure that the generated projection data

and images are visually realistic. It should be noted that, during the training process, it is crucial to consider the weight balance among different loss functions. To capture the nonlocal features, Wang et al. [27] introduced the vision transformer [116] into the sinogram network to enhance the long-range dependency modeling capability.

In IT, projection data are often contaminated by many factors, such as photon scattering and small-sized detectors. Han et al. [64] found that the image domain networks could not effectively deal with coupled artifacts, since they did not satisfy the low-rank property. Therefore, they introduced a sinogram domain network to deal with the noise for the measured projection data, and the image domain network refine the image quality. Chen et al. [65] and Ketola et al. [66] adopted similar solutions. Ketola et al. further introduced two generative adversarial networks (GANs) into the dual-domain networks to improve the sinogram restoration and visual results.

Similarly, in MAR, Lin et al. [29] proposed an end-to-end dual-domain neural network (DuDoNet) to restore projection data and correct CT images simultaneously. DuDoNet regarded the metal-affected projection data as missing data and filled them with the estimated data. Therefore, fine-grained details may be ignored and the reconstructed images may be over-smoothed. To retain more details, Lyu et al. [67] proposed DuDoNet++, which took the original metal-affected projection data and the corresponding reconstruction as inputs. DuDoNet++ further explicitly fed the metal projection information to each stage of the projection domain network for capturing metal geometric information. However, Yu et al. [60] argued that there would be minor anatomical changes when the output of the image domain network was regarded as the final corrected results. Thus, they reversed the processing order of two domains, where the two subnetworks were connected with a differentiable forward projection layer. The final corrected CT image was reconstructed from the output sinogram.

These dual-domain methods generally processed data in a specific serial processing order, which implicitly imposed a certain priority on the domains and ignore the potential information interaction between two domains. To address this problem, Wang et al. [68] proposed an interactive dual-domain parallel network for MAR to fully use the information interaction between two domains. Gao et al. [69] designed a dual-domain attention-based deep network. The dual-domain network worked in parallel and the features from the two domains were fused with hybrid attention modules at different scales, thus enhancing the interaction between the dual domains.

Although these methods are effective in suppressing artifacts to some extent, they do not explicitly guarantee the consistency of the projected data. Some researchers have borrowed solutions from traditional iterative reconstruction methods. Iterative methods follow the process of calculating the difference between the projected data of the estimated image. This difference is then back-projected into the image domain to generate a residual image, which is subsequently employed to update the intermediate estimated image, iteratively. Thus,

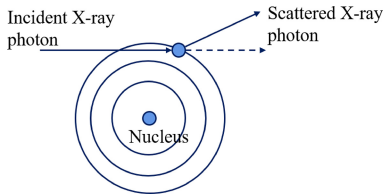


Fig. 3. Diagrammatic sketch of scatter.

the corrected image tends to be consistent with the measured projection data. Inspired by this, Hu et al. [70] and Chen et al. [71] used neural networks to imitate the iterative algorithm for consistency. A more general way is to employ a projection data fidelity layer [60], [68], [72] for focusing on the inpainting of missing data in the sinogram domain. In these works, the measured projection data outside the metal trace is regarded as reliable and retained. Then the projection data estimated by the trained network was used to fill in the missing projection. Considering that the projection data inside and outside the metal trace obey different distributions, Wang et al. [72] employed a residual learning strategy to avoid converting the two distribution data into the same one, thus easing the network learning.

However, in reality, X-rays can scatter when they interact with body tissues. This leads to the deflection of incident photons, as depicted in Fig. 3, and inaccuracies in the detected signal and ultimately affecting the accuracy of the CT reconstruction. To address this problem, Zhou et al. [31] designed a novel projection data fidelity layer. In their work, the combination of estimated and measured data based on the projection domain mask is not a straightforward process. They merged the network's output and measured projection data by a weighting technique while taking into account the sinogram's noise level to obtain an accurate correction result. However, the drawback is that the weight is manually assigned and does not adapt dynamically based on the input projection data.

Dual-domain methods have access to both raw projection data and images, resulting in reconstructed images of superior quality compared to single-domain methods. Due to its impressive artifact reduction performance, the dual-domain method has emerged as the mainstream for CT reconstruction from incomplete projection data.

4) Domain Transformation Learning: The aforementioned sinogram and dual-domain methods generally used analytical reconstruction algorithms, such as FBP. However, FBP requires complete projection data, otherwise, the reconstructed CT images will contain artifacts. Over the past few years, DL has become a potent technique to map the captured projection data directly to the image domain, without depending on mathematical models, which is recognized as a domain transformation process. For instance, Zhu et al. [73] presented a unified reconstruction framework for domain transformation using manifold approximation (AUTOMAP). Although a good potential for end-to-end reconstruction has been shown in AUTOMAP, the performance of the model was constrained by a substantial number of parameters in the stacked fully connected (FC) layers, which was not clinically

applicable. To address this problem, Fu and De Man [74] considered the problem as a series of simpler subproblems and proposed to implement domain transformation gradually in a hierarchical manner, thereby reducing the parameter number.

Similarly, Li et al. [75] developed iCT-Net by leveraging the classical FBP algorithm. This innovative approach utilizes networks to perform various stages of FBP. Specifically, the first few layers of the network repair the sinogram, while subsequent layers mimic the filtering and back-projection process, respectively. In contrast to iCT-Net, which employs a fixed filter setting, He et al. [76] utilized FC filtering to adaptively filter the projection data. However, the same problem is encountered again; this approach demands a significant number of trainable parameters in FC and results in high-memory consumption. To alleviate this issue, Kandarpa et al. [77] proposed a trainable fully convolution layer and achieved near-instantaneous reconstruction. To improve the reconstruction performance, Kandarpa et al. [78] further proposed a U-Net-like end-to-end framework. The features at the encoding stage were reused for the decoding stage. The success of the decoding stage mainly depended on the task-specific concatenations generated from down-sampled inputs. In instances where down-sampled inputs were not accessible, the domain transformation task was insufficiently performed. This led to the appearance of white dots arranged in a particular pattern in the reconstructed images.

Domain transformation learning offers a significant advantage, as it allows the neural network to dynamically learn the reconstruction parameters based on the input projection data. This approach has demonstrated remarkable potential and is expected to remain an active field of research.

B. Unsupervised and Semi-Supervised Learning

The aforementioned methods used supervised learning that requires a substantial amount of paired data for learning the mapping from uncorrected data to corrected data. However, obtaining paired training data could be challenging in real-world scenarios. To address this problem, semi-supervised [79], [80], [81], [82], [83] and unsupervised [84], [85], [86], [87] methods have been investigated. For example, Zhou et al. [79] adopted two generators to learn the mapping between real and simulated sinogram. Then, the clinical data could be converted and participated in the artifact reduction process as simulated sinogram. Zhao et al. [85] proposed two modes for sinogram inpainting. In cases where ground truth was not available, such as in a clinical scenario, they minimized the loss between the measured sinogram and the counterpart section of the model's outputs. Inspired by the deep image prior (DIP) [88], Wu et al. [89] integrated it with the vision transformer [90] to develop an untrained transformer model for SV cone beam CT reconstruction, where only the corrupted images are available.

With regard to MAR, due to the domain gap between synthetic data and clinical data, supervised methods usually do not perform well in clinical applications. To overcome this challenge, unsupervised MAR methods were proposed as

an alternative approach. Liao et al. [80] proposed to disentangle metal-affected images into distinct latent spaces with specialized loss functions. However, this approach relied on a complicated artifact decoupling process implemented by a complex network structure. Lee et al. [86] used U-Net with only two-step downsampling as the generator and learned the mappings between the metal-corrupted and the metal-free domain directly. Hence, the network structure and disentanglement procedure are much simpler than those of ADN, resulting in fewer parameters and promoting its clinical application. Furthermore, they drew inspiration from β -VAE [91] and introduced a controllable parameter, β , in the loss function to enhance the interpretability of the disentanglement process.

Despite significant efforts, unsupervised methods have shown limited improvement in MAR performance, especially in scenarios with heavy artifacts. On the other hand, simulated data, while not capable of fully capturing the complexity of clinical scenarios, can provide valuable information about anatomical structures through strong supervision [92]. Niu et al. [82] and Shi et al. [81] have devised a hybrid training approach that leverages both advantages of supervised and unsupervised methods. They used paired simulated data and unpaired clinical data during the training process with the same networks. By combining these techniques, more robust and accurate results were achieved. Unlike these methods, which trained the model with simulated and clinical data simultaneously, Lyu et al. [83] utilized a pretrained sinogram domain network that had been trained on a simulated dataset to assist in the restoration of real sinograms. In the clinical study, more tissue details were preserved in these semi-supervised methods compared with unsupervised methods.

Unsupervised and semi-supervised DL-based methods have shown promising results for addressing artifact reduction in CT reconstruction from incomplete projection data. These methods can learn the underlying patterns and features of the data with limited or without the need for explicit supervision, which is particularly useful in cases where labeled data is scarce or expensive to obtain.

IV. EVALUATION

A. Dataset

1) *DeepLesion*: The DeepLesion dataset [98] was developed by the National Institutes of Health Clinical Center (NIHCC). It contains a vast collection of over 32 000 images depicting different pathological conditions, including kidney lesions, bone lesions, pulmonary nodules, and lymph node enlargement. The dataset is extensive and comprehensive, featuring bounding boxes and size measurements for each lesion, making it an ideal resource for medical image analysis and computer-aided diagnosis.

2) *SpineWeb Dataset 3*: The Department of Radiology at the University of Washington has made available the SpineWeb Dataset 3 [99] for the purpose of vertebrae localization and identification. It includes CT scans of 125 patients with various spinal pathologies, and a total of 242 scans are available due to longitudinal examinations. Notably, this dataset includes CT images with clinical metal artifacts.

3) *AAPM*: This dataset [100] comprised various types of lesions, including subtle and typical ones. Patient data of varying sizes were incorporated into the dataset for training. For both patient and phantom data, full-dose and quarter-dose FBP images with lesion locations were provided along with the corresponding projection data.

4) *CTPelvic1K*: The dataset [101] consists of 1184 CT volumes of the pelvis, comprising over 320 000 slices obtained from multiple sources and manufacturers. These slices exhibit varying resolutions and appearances, making the dataset diverse and comprehensive. This dataset includes 1109 CT volumes free of metal artifacts and 75 CT volumes affected by metal artifacts.

B. Deep Reconstruction Tools

Projection and reconstruction operations lead to high-computational and memory costs. However, this issue can be relieved by utilizing CUDA-accelerated toolkits. These toolkits facilitate the implementation of optimized CUDA kernels for projection and reconstruction operations, exploiting the full computing capabilities of contemporary GPUs. Moreover, these toolkits can seamlessly integrate with the PyTorch automatic derivation mechanism. Therefore, the projection and reconstruction layers can be incorporated into the network and trained jointly.

1) *ASTRA Toolbox*: ASTRA Toolbox¹ offers support for 2-D parallel and fan beam geometries, as well as 3-D parallel and cone beam geometries, all with highly adaptable source and detector positioning capabilities. Additionally, its fundamental forward and backward projection operations can be accelerated by GPU, providing users with the necessary tools to develop their own custom algorithms.

2) *ODL*: The Operator Discretization Library (ODL)² is a Python library that can quickly solve inverse problems. The analytic or iterative reconstruction methods used in CT imaging are essentially processes of inverse function calculation. The *tomo* module in the ODL library can effectively solve 2-D/3-D CT image reconstruction problems and can be accelerated using GPUs.

3) *TorchRadon*: TorchRadon [102] is a PyTorch extension for solving CT reconstruction problems, which provides differentiable routines, such as forward and back projections and shearlet transforms. It operates up to 125× faster than the ASTRA Toolbox and supports batch operations, transparent API, and half-precision.

4) *NeuTomPy Toolbox*: The NeuTomPy toolbox [103] is a Python software package used for tomographic data processing and reconstruction. This toolbox includes preprocessing algorithms, artifact removal, and extensive iterative reconstruction methods, as well as the FBP algorithm. The NeuTomPy toolbox was originally designed for neutron tomography, aiming to meet the needs of users and researchers to compare the latest reconstruction methods and select the best-data processing workflow for their data.

¹<https://github.com/astra-toolbox/astra-toolbox>

²<https://github.com/odlgroup/odl>

TABLE II
QUANTITATIVE RESULTS OF DIFFERENT METHODS FOR SV, LA, IT AND RING ARTIFACT REDUCTION ON THE SIMULATED DATASET

Methods	SV		LA		IT		Ring artifact reduction	
	PSNR	SSIM	PSNR	SSIM	PSNR	SSIM	PSNR	SSIM
FBP	20.93	0.6391	25.95	0.4697	23.73	0.6398	33.78	0.8696
DD-Net	47.24	0.9877	41.99	0.9791	36.48	0.9521	43.10	0.9836
DCAR	45.56	0.9874	43.26	0.9570	42.67	0.9714	45.84	0.9886
FBPConvNet	50.18	0.9936	42.99	0.9601	43.00	0.9785	51.36	0.9975
Framing_Net	48.30	0.9940	40.32	0.9807	42.60	0.9671	44.67	0.9878
LRR-CED	46.53	0.9878	37.91	0.9673	43.96	0.9850	41.64	0.9779
HD-Net	47.19	0.9839	43.61	0.9693	45.78	0.9889	43.04	0.9846

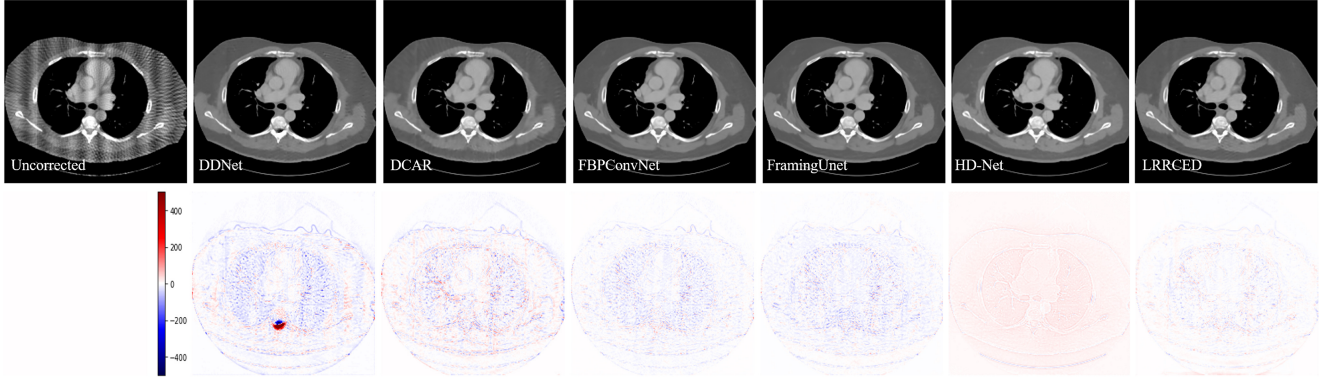


Fig. 4. Visual results of different methods for SV on the simulated dataset. The sampling rate is 1/4. Display window: [−375, 560] HU.

5) *CTLib*: *CTLib*³ is a Library of CT projector and back-projector based on PyTorch. One limitation of this approach is that it only utilizes 2-D projection data, which may restrict its applications in certain scenarios.

6) *TomoPy Toolbox*: *TomoPy*⁴ contains a range of image reconstruction algorithms that are used for tomography. It also includes several filters, ring removal algorithms, and phase retrieval algorithms that help to enhance the quality of the reconstructed CT images.

C. Artifacts Reduction Performance

In this section, we evaluated the performance of the recent state-of-the-art methods for SV, LA, IT and ring artifacts reduction, including Jin et al. [25] (denoted as FBPConvNet), Han and Ye [56] (denoted as Framing-Unet), Zhang et al. [55] (denoted as DD-Net), Huang et al. [51] (denoted as DCAR), Kandarpa et al. [78] (denoted as LRR-CED), and Hu et al. [104] (denoted as HD-Net). The DL-based methods for SV reconstruction were trained on simulated data with an under-sampling rate of four. For LA reconstruction, the training data was sampled at the range of [0°, 120°]. In IT reconstruction, only 32% of detectors can receive data. In ring artifacts reduction, 30 broken pixels of the detector are randomly spaced with inconsistent gain at [0.95, 1.05].

The average PSNR and SSIM scores are listed in Table II. From the table, we can observe that U-Net-based (FBPConvNet, Framing-UNet, and DCAR) methods achieved impressive artifact reduction performance in SV, LA, and IT, which shows the effectiveness of U-Net-like architecture. The

domain transformation method LRRCED also shows impressive performance. It is worth noting that, the dual-domain method HD-Net achieves the best-PSNR and SSIM scores in IT reconstruction and the best-PSNR score in LA reconstruction, which demonstrates the advantages of hybrid-domain methods. For visual comparison, Figs. 4–7 illustrate the artifact reduction performance of these DL-based methods for LA, SV, IT and ring artifacts reduction, respectively. The residual between the ground truth and the corrected results is also provided.

For MAR, several state-of-the-art DL-based MAR methods were evaluated, including Liao et al. [80] (denoted as ADN), Lyu et al. [67] (denoted as DuDoNet++), Yu et al. [60] (denoted as DSCIP), Yu et al. [105] (denoted as SSCMAR), Wang et al. [68] (denoted as IDOL-Net), and Lyu et al. [83] (denoted as U-DuDoNet). Table III presents the average PSNR and SSIM scores on the simulated dataset. Fig. 8 shows representative results of these methods with different metal sizes. For better visualization, the metals are painted in red. It can be observed that all methods significantly improved imaging quality compared with uncorrected CT images, in terms of both quantitative analysis and visual comparison. Moreover, DuDoNet++, DSCIP, and SSCMAR obtained better performance on synthesized dataset, which shows the superiority of dual-domain supervised methods, since they leveraged information in both the sinogram domain and image domain.

To verify the generalization of these investigated MAR methods in a clinical scenario, we applied these models trained on the synthetic dataset on clinical CT images with realistic metal artifacts from the SpineWeb dataset [99]. Fig. 9 presents visual results. Similar to DAN-Net and DSCIP, the metals were segmented using 2000 HU as the threshold and painted in red. Although the supervised dual-domain method

³<https://github.com/xwj01/CTLIB>

⁴<https://github.com/tomopy/tomopy>

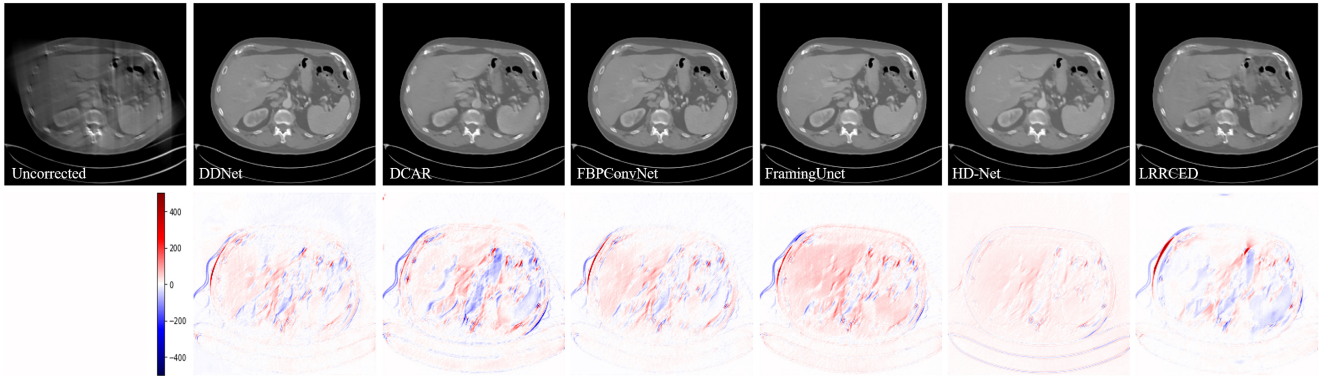


Fig. 5. Visual results of different methods for LA on the simulated dataset. The sampling range: $[0^\circ, 120^\circ]$. Display window: $[-375, 560]$ HU.

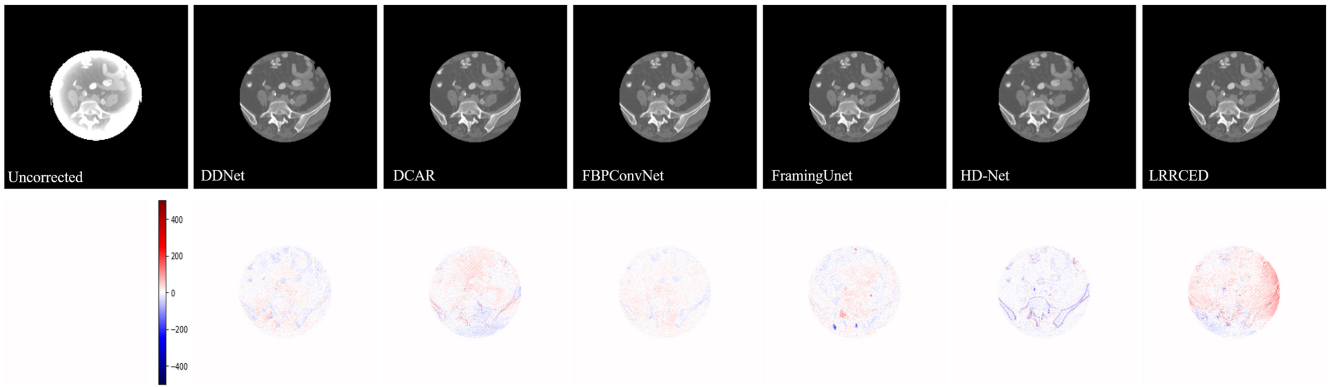


Fig. 6. Visual results of different methods for IT on the simulated dataset. Truncation rate is 0.68. Display window: $[-375, 560]$ HU.

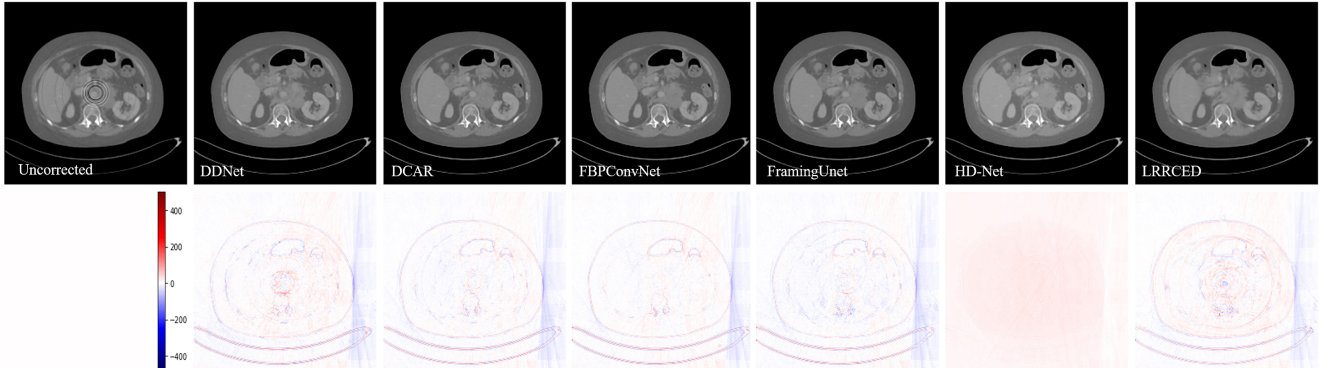


Fig. 7. Visual results of different methods for ring artifacts reduction on the simulated dataset. The broken detector number is 30. Display window: $[-375, 560]$ HU.

TABLE III
QUANTITATIVE RESULTS OF DIFFERENT MAR
METHODS ON THE SIMULATED DATASET

Methods	PSNR(dB)	SSIM
FBP	18.93	0.7935
ADN	30.58	0.9290
DuDOnet++	37.65	0.9770
DSCIP	38.19	0.9635
SSCMAR	34.87	0.9285
IDOL-Net	41.57	0.9880
U-DuDOnet	34.54	0.9340

achieved excellent qualitative scores and visual results on the simulated dataset, their corrected results on the clinical dataset appeared over-smooth. On the contrary, unsupervised

and semi-supervised methods yielded better preservation of bone details.

D. Stability Performance

Stability in DL refers to the ability of a DL-based model to consistently produce accurate results despite variations in the input data [106]. We use testing data with different sampling rates from the training dataset to test the stability of the models. In Figs. 10 and 11, the models are trained on data with a sampling rate of 1/4 and were tested with the sampling rate of 1/6 and 1/2, respectively. In Figs. 13 and 12, the models were trained on data with the sampling range at $[0^\circ, 120^\circ]$ and

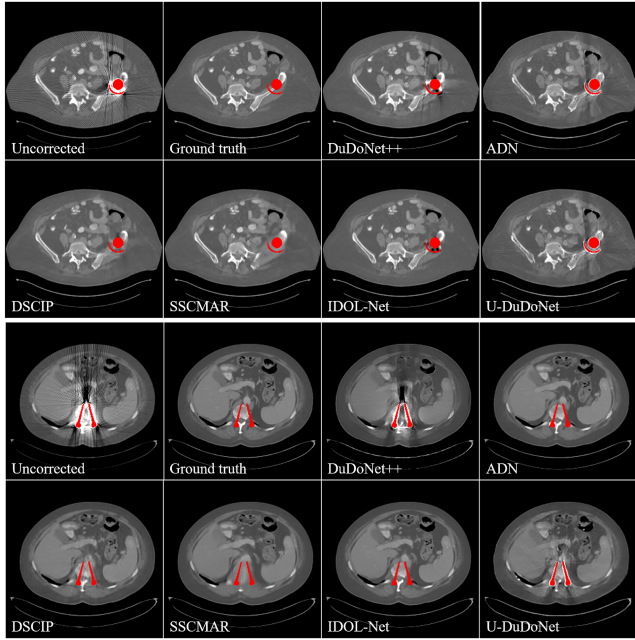


Fig. 8. Visual results of different MAR methods on the simulated dataset. Display window: [−375, 560] HU.

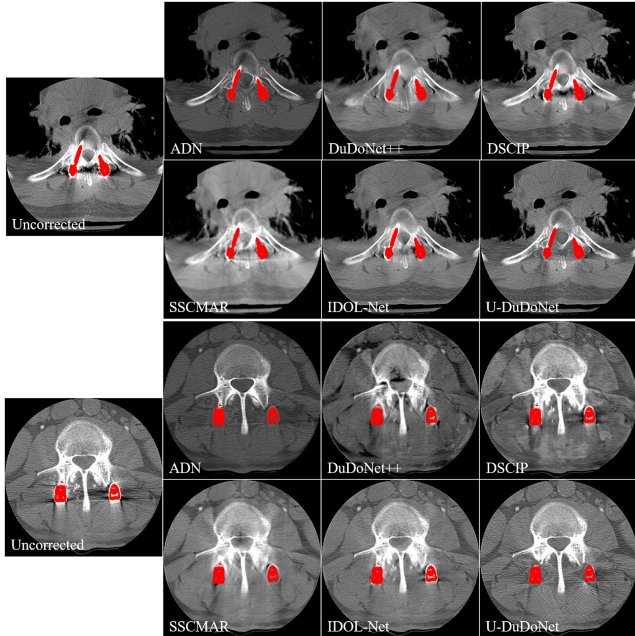


Fig. 9. Visual results of different MAR methods on the clinical dataset. Display window: [−375, 560] HU.

were tested with the sampling range at $[0^\circ, 150^\circ]$ and $[0^\circ, 90^\circ]$, respectively. In Figs. 15 and 14, the models were trained on data with a truncation rate of 0.68 and were tested with truncation rates of 0.72 and 0.58, respectively. In Figs. 16 and 17, the numbers of broken detector units are 50 and 10, respectively. It is noticeable that when the completeness of the test data in the projection data is higher than that of the training data, the models' performance can generally be preserved. However, if the incompleteness of the test data in the projection data exceeds that of the training data, the models' performance may be degraded.

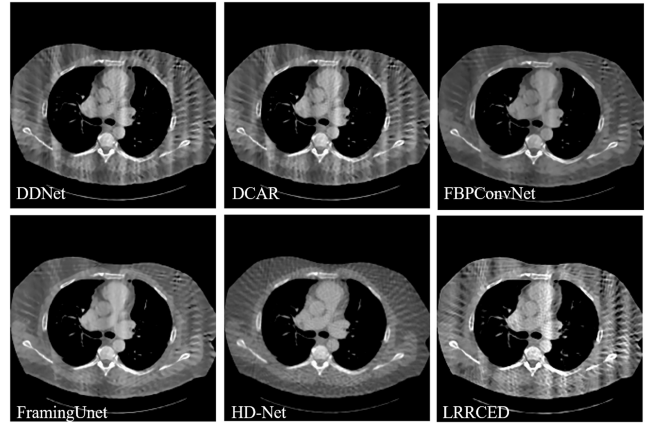


Fig. 10. Visual results of different methods for SV on the simulated dataset. The sampling rate is 1/6. The models are trained on data with a sampling rate of 1/4 in Fig. 4. Display window: [−375, 560] HU.

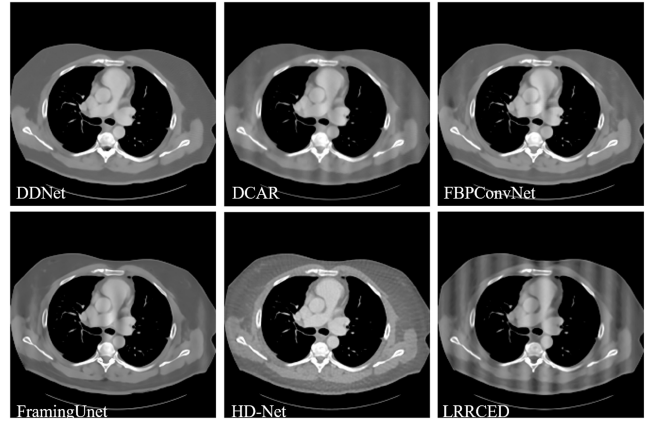


Fig. 11. Visual results of different methods for SV on the simulated dataset. The sampling rate is 1/2. The models are trained on data with a sampling rate of 1/4 in Fig. 4. Display window: [−375, 560] HU.

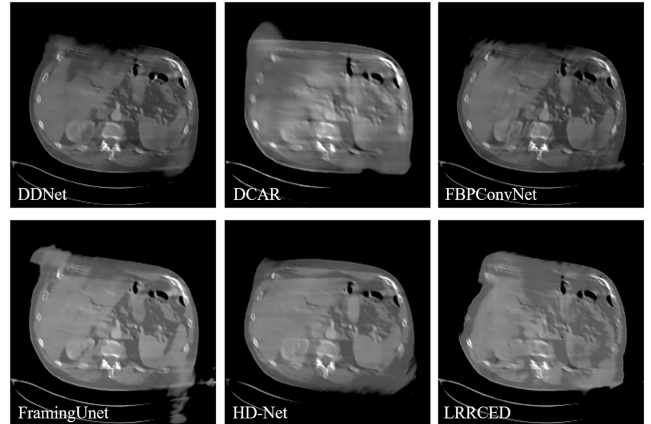


Fig. 12. Visual results of different methods for LA on the simulated dataset. The sampling range is $[0^\circ, 90^\circ]$. The models are trained on data with the sampling range at $[0^\circ, 120^\circ]$ in Fig. 5. Display window: [−375, 560] HU.

V. CONCLUSION AND FUTURE WORKS

With the emergence of DL, DL-based reconstruction methods have been developed for tomographic imaging. In this survey, we present a comprehensive review of DL-based CT reconstruction techniques for incomplete projection data over the past decade, for the problems, including SV, LA, MAR, IT, and

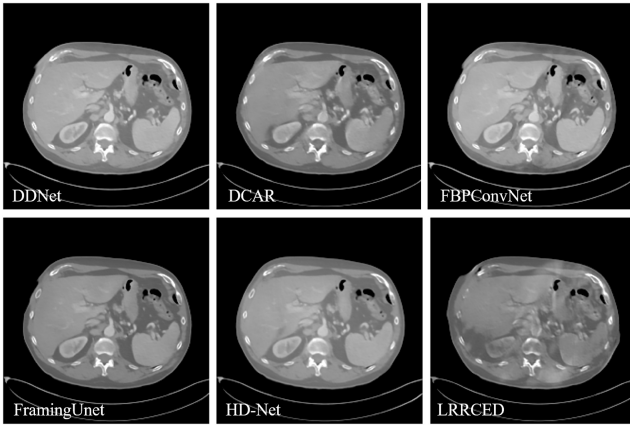


Fig. 13. Visual results of different methods for LA on the simulated dataset. The sampling range is $[0^\circ, 150^\circ]$. The models are trained on data with the sampling range at $[0^\circ, 120^\circ]$ in Fig. 5. Display window: $[-375, 560]$ HU.

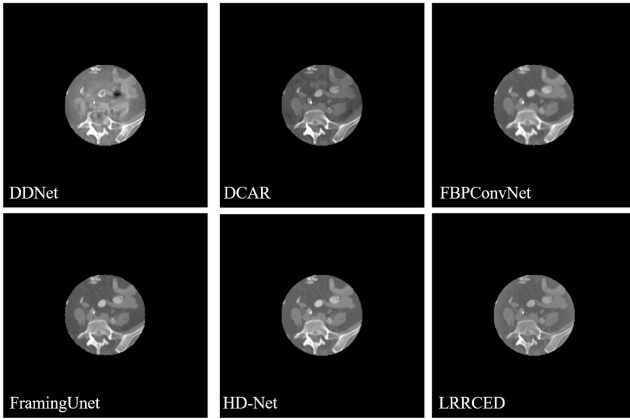


Fig. 14. Visual results of different methods for IT on the simulated dataset. The truncation rate is 0.58. The models are trained on data with a truncation rate of 0.68 in Fig. 6. Display window: $[-375, 560]$ HU.

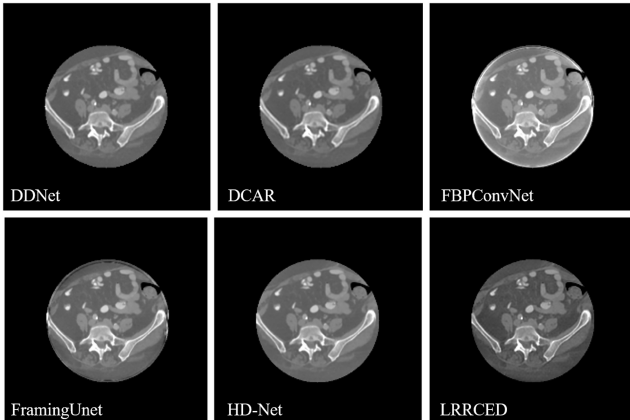


Fig. 15. Visual results of different methods for IT on the simulated dataset. The truncation rate is 0.72. The models are trained on data with a truncation rate of 0.68 in Fig. 6. Display window: $[-375, 560]$ HU.

ring artifacts reduction reconstruction problems. Despite the promising results achieved by these DL-based methods, there are still several potential limitations that need to be addressed.

Data Simulation: Due to the complex physical process involved in CT imaging, it is not feasible for a simulated dataset to cover all scenarios. For instance, in the case of

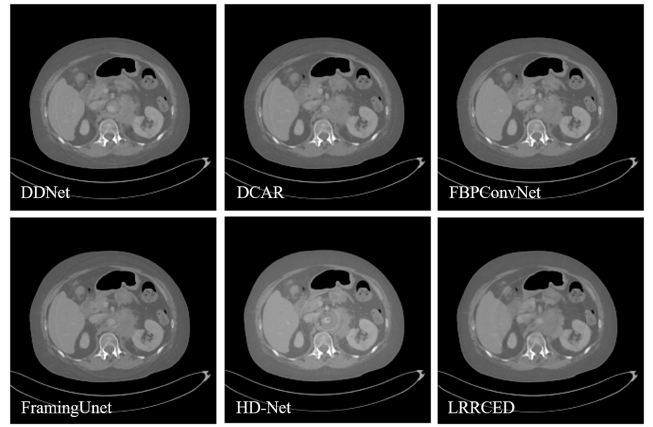


Fig. 16. Visual results of different methods for ring artifacts reduction on the simulated dataset. The number of broken detectors is 50. The models are trained on data with the number of broken detectors at 30 in Fig. 7. Display window: $[-375, 560]$ HU.

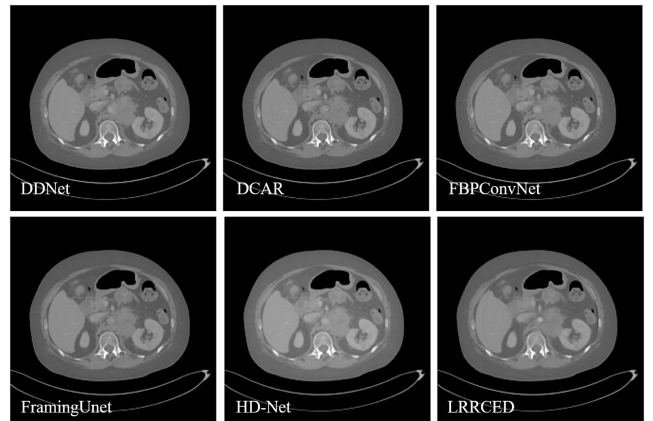


Fig. 17. Visual results of different methods for ring artifacts reduction on the simulated dataset. The number of broken detectors is 10. The models are trained on data with the number of broken detectors at 30 in Fig. 7. Display window: $[-375, 560]$ HU.

MAR, the impact of various phenomena, such as noise, photon starvation, beam hardening, scattered radiation, and non-linear partial volume effects, can be exacerbated by metallic objects, which cannot be simulated with a straightforward configuration.

Model Deployment: Deploying DL models for CT reconstruction poses several challenges, such as the high-computational and memory costs of training and inference with complex models, optimizing models for efficient implementation on the hardware, and ensuring that deployed models can handle data obtained from different acquisition parameters while providing real-time accurate results. In addition, in practical applications, reconstruction algorithms are more challenging to deploy than post-processing methods that only require CT images as input, since they need access to projection data.

Lacking Domain Knowledge: The projection domain methods are more akin to image inpainting tasks, while image domain methods resemble image denoising tasks. However, the imaging principles of CT and natural images are fundamentally different, and there is a lack of in-depth exploration of domain-specific knowledge for CT imaging. Moreover,

most neural networks used for CT reconstruction with incomplete projection are black boxes, lacking interpretability that can be convincing for clinical practice. The absence of interpretability poses difficulty in comprehending the reasoning behind the neural network's outcomes and assessing its efficacy, thereby creating a hindrance. Hence, it is crucial to investigate novel techniques that improve the explainability of neural networks in CT reconstruction and to bridge the gap between domain knowledge and the design of neural networks.

Reconstructing high-quality CT images from incomplete projection data remains challenging in the field of medical imaging. Although there have been noteworthy improvements in this field, the matter is still far from being completely resolved. To address the challenges, several potential directions have been suggested, which are worth exploring further.

Benchmark Dataset: DL required a large number of training data while there is no benchmark dataset for incomplete projection data reconstruction. Different methods are developed using different synthetic or clinical CT data, and the comparison results are not intuitive. Therefore, establishing a benchmark dataset for incomplete projection data reconstruction is of great urgency.

Combining Diagnostics Purposes: While it is essential to achieve good quantitative scores, such as high resolution and low noise, these metrics are not the ultimate goal. In fact, the target is to provide doctors with accurate and useful images that can aid them in making diagnoses and developing treatment plans. Thus, it is crucial to develop task-specific imaging methods, that focus on tailoring CT reconstruction to a specific clinical application. Such approaches take into account the specific needs of the doctor and the patient and can help improve diagnostic accuracy. For example, in CT imaging after an operation of cerebral aneurysms, doctors only focus on the situation of blood vessels near the metal. Other parts, no matter how well they are reconstructed, cannot provide doctors with good references. Therefore, task-specific imaging is worth exploring in future research.

Self-Supervised Learning: DL-based methods have shown great potential in CT image reconstruction, where the optimization process often requires a reference set of data to train the model. However, obtaining a well-matched, uncorrected CT image and its corresponding corrected version, is often challenging in clinical settings. Recently, self-supervised learning which does not rely on extra annotations, has shown remarkable progress in various domains. Efforts have been made to develop self-supervised learning methods for image denoising. For example, Noise2Void [107] and Noise2Self [108] are typical methods that predict each center pixel from its local neighbors, achieving promising results with only noisy images under the assumption of independent noises among neighbor pixels. In CT reconstruction, some self-supervised learning methods have also been proposed [109], [110]. These methods leverage the inherent structure and information present in the data itself to learn denoising models. They are effective in capturing local and statistical properties of the noise and image content. Thus, incorporating self-supervised learning into CT reconstruction

with incomplete projection data could be a valuable research direction.

Federated Learning (FL): Due to the sensitivity of medical data, it is difficult to centralize a large number of CT scan datasets for processing. FL can train these data without revealing them, thus protecting the privacy of medical data. In addition, FL can also help solve the problem of data imbalance. In CT reconstruction, due to differences in patient conditions and CT equipment, data often exhibits imbalance. FL can train and exchange information between different devices, thus improving the model's generalization ability and stability. FL has a wide range of application prospects in CT reconstruction, which is an interesting work to explore.

Diffusion Models: Diffusion-based models are a class of generative models that have shown great success in image-denoising tasks. The approach consists of a diffusion process that iteratively transforms a noise distribution to the target image distribution. The diffusion process is controlled by a set of learnable parameters that are optimized using maximum likelihood estimation. Once the parameters are learned, the model can be used to generate denoised images by sampling from the diffusion process. In CT reconstruction, diffusion-based models have been employed to denoise the sinogram [111], [112], [113] CT images directly [114], [115]. They have shown promising results in CT reconstruction, achieving state-of-the-art performance in several benchmarks. However, they are computationally expensive, thus challenging to deploy in clinical settings. Therefore, there is still a need for more efficient and scalable diffusion-based denoising methods for CT reconstruction.

ACKNOWLEDGMENT

All authors declare that they have no known conflicts of interest in terms of competing for financial interests or personal relationships that could have an influence or are relevant to the work reported in this article.

REFERENCES

- [1] R. A. Brooks, G. H. Weiss, and A. J. Talbert, "A new approach to interpolation in computed tomography," *J. Comput. Assist. Tomogr.*, vol. 2, no. 5, pp. 577–585, 1978.
- [2] R. M. Lewitt and R. Bates, "Image reconstruction from projections III: Projection completion methods," *Optik*, vol. 50, no. 3, pp. 189–204, 1978.
- [3] M. Bertram, J. Wiegert, D. Schafer, T. Aach, and G. Rose, "Directional view interpolation for compensation of sparse angular sampling in cone-beam CT," *IEEE Trans. Med. Imag.*, vol. 28, no. 7, pp. 1011–1022, Jul. 2009.
- [4] H. Zhang and J.-J. Sonke, "Directional sinogram interpolation for sparse angular acquisition in cone-beam computed tomography," *J. X-Ray Sci. Technol.*, vol. 21, no. 4, pp. 481–496, 2013.
- [5] Y. Lu, J. Zhao, and G. Wang, "Few-view image reconstruction with dual dictionaries," *Phys. Med. Biol.*, vol. 57, no. 1, p. 173, 2011.
- [6] H. Yu and G. Wang, "A soft-threshold filtering approach for reconstruction from a limited number of projections," *Phys. Med. Biol.*, vol. 55, no. 13, p. 3905, 2010.
- [7] S. Li, Q. Cao, Y. Chen, Y. Hu, L. Luo, and C. Toumoulin, "Dictionary learning based sinogram inpainting for CT sparse reconstruction," *Optik*, vol. 125, no. 12, pp. 2862–2867, 2014.
- [8] D. Karimi and R. Ward, "Reducing streak artifacts in computed tomography via sparse representation in coupled dictionaries," *Med. Phys.*, vol. 43, no. 3, pp. 1473–1486, 2016.

- [9] Y. Gao et al., "A feasibility study of extracting tissue textures from a previous full-dose CT database as prior knowledge for Bayesian reconstruction of current low-dose CT images," *IEEE Trans. Med. Imag.*, vol. 38, no. 8, pp. 1981–1992, Aug. 2019.
- [10] A. Chambolle and P.-L. Lions, "Image recovery via total variation minimization and related problems," *Numer. Math.*, vol. 76, no. 2, pp. 167–188, 1997.
- [11] Q. Xu, H. Yu, X. Mou, L. Zhang, J. Hsieh, and G. Wang, "Low-dose X-ray CT reconstruction via dictionary learning," *IEEE Trans. Med. Imag.*, vol. 31, no. 9, pp. 1682–1697, Sep. 2012.
- [12] W. Wu, F. Liu, Y. Zhang, Q. Wang, and H. Yu, "Non-local low-rank cube-based tensor factorization for spectral CT reconstruction," *IEEE Trans. Med. Imag.*, vol. 38, no. 4, pp. 1079–1093, Apr. 2019.
- [13] G. Wang, Y. Zhang, X. Ye, and X. Mou, *Machine Learning for Tomographic Imaging*. Bristol, U.K.: IOP Publ., 2019.
- [14] W. Xia et al., "Magic: Manifold and graph integrative convolutional network for low-dose CT reconstruction," *IEEE Trans. Med. Imag.*, vol. 40, no. 12, pp. 3459–3472, Dec. 2021.
- [15] Y. Huang et al., "Noise-powered disentangled representation for unsupervised speckle reduction of optical coherence tomography images," *IEEE Trans. Med. Imag.*, vol. 40, no. 10, pp. 2600–2614, Oct. 2021.
- [16] H. Chen et al., "Low-dose CT with a residual encoder-decoder convolutional neural network," *IEEE Trans. Med. Imag.*, vol. 36, no. 12, pp. 2524–2535, Dec. 2017.
- [17] Z. Lu et al., "M3NAS: Multi-scale and multi-level memory-efficient neural architecture search for low-dose CT denoising," *IEEE Trans. Med. Imag.*, vol. 42, no. 3, pp. 850–863, Mar. 2023.
- [18] J. Lu, F. Millioz, D. Garcia, S. Salles, W. Liu, and D. Friboulet, "Reconstruction for diverging-wave imaging using deep convolutional neural networks," *IEEE Trans. Ultrason. Ferroelectr. Freq. Control*, vol. 67, no. 12, pp. 2481–2492, Dec. 2020.
- [19] J. Dong, J. Fu, and Z. He, "A deep learning reconstruction framework for X-ray computed tomography with incomplete data," *Plos One*, vol. 14, no. 11, 2019, Art. no. e0224426.
- [20] Y. Zhang et al., "LEARN++: Recurrent dual-domain reconstruction network for compressed sensing CT," *IEEE Trans. Radiat. Plasma Med. Sci.*, vol. 7, no. 2, pp. 132–142, Feb. 2023.
- [21] G. Wang, J. C. Ye, and B. De Man, "Deep learning for tomographic image reconstruction," *Nat. Mach. Intell.*, vol. 2, no. 12, pp. 737–748, 2020.
- [22] X. Dong, S. Vekhande, and G. Cao, "Sinogram interpolation for sparse-view micro-CT with deep learning neural network," in *Proc. Phys. Med. Imag.*, 2019, pp. 692–698.
- [23] H. Lee, J. Lee, H. Kim, B. Cho, and S. Cho, "Deep-neural-network-based sinogram synthesis for sparse-view CT image reconstruction," *IEEE Trans. Radiat. Plasma Med. Sci.*, vol. 3, no. 2, pp. 109–119, Mar. 2019.
- [24] M. U. Ghani and W. C. Karl, "Deep learning based sinogram correction for metal artifact reduction," *Electron. Imag.*, vol. 30, no. 15, p. 472, 2018.
- [25] K. H. Jin, M. T. McCann, E. Froustey, and M. Unser, "Deep convolutional neural network for inverse problems in imaging," *IEEE Trans. Image Process.*, vol. 26, pp. 4509–4522, 2017.
- [26] S. Guan, A. A. Khan, S. Sikdar, and P. V. Chitnis, "Fully dense UNet for 2-D sparse photoacoustic tomography artifact removal," *IEEE J. Biomed. Health Inform.*, vol. 24, no. 2, pp. 568–576, Feb. 2020.
- [27] C. Wang, K. Shang, H. Zhang, Q. Li, Y. Hui, and S. K. Zhou, "DuDoTrans: Dual-domain transformer provides more attention for sinogram restoration in sparse-view CT reconstruction," 2021, *arXiv:2111.10790*.
- [28] Y. Zhang et al., "CD-Net: Comprehensive domain network with spectral complementary for DECT sparse-view reconstruction," *IEEE Trans. Comput. Imag.*, vol. 7, pp. 436–447, 2021.
- [29] W.-A. Lin et al., "DuDoNet: Dual domain network for CT metal artifact reduction," in *Proc. IEEE Conf. Comput. Vis. Pattern Recognit.*, 2019, pp. 10512–10521.
- [30] B. Zhou, X. Chen, S. K. Zhou, J. S. Duncan, and C. Liu, "DuDoDR-net: Dual-domain data consistent recurrent network for simultaneous sparse view and metal artifact reduction in computed tomography," *Med. Image Anal.*, vol. 75, Jan. 2022, Art. no. 102289.
- [31] B. Zhou, S. K. Zhou, J. S. Duncan, and C. Liu, "Limited view tomographic reconstruction using a cascaded residual dense spatial-channel attention network with projection data fidelity layer," *IEEE Trans. Med. Imag.*, vol. 40, no. 7, pp. 1792–1804, Jul. 2021.
- [32] F. P. Vidal, J. M. Létang, G. Peix, and P. Cloetens, "Investigation of artefact sources in synchrotron microtomography via virtual X-ray imaging," *Nucl. Instrum. Methods. Phys. Res. B*, vol. 234, no. 3, pp. 333–348, 2005.
- [33] S. Chang, X. Chen, J. Duan, and X. Mou, "A CNN-based hybrid ring artifact reduction algorithm for CT images," *IEEE Trans. Radiat. Plasma Med. Sci.*, vol. 5, no. 2, pp. 253–260, Mar. 2021.
- [34] Y. Liu, C. Wei, and Q. Xu, "Detector shifting and deep learning based ring artifact correction method for low-dose CT," *Med. Phys.*, vol. 50, no. 7, pp. 4308–4324, 2023.
- [35] O. Ronneberger, P. Fischer, and T. Brox, "U-Net: Convolutional networks for biomedical image segmentation," in *Proc. Int. Conf. Med. Image Comput. Assist. Intervent.*, 2015, pp. 234–241.
- [36] K. He, X. Zhang, S. Ren, and J. Sun, "Deep residual learning for image recognition," in *Proc. IEEE Conf. Comput. Vis. Pattern Recognit.*, 2016, pp. 770–778.
- [37] S. Li, W. Ye, and F. Li, "LU-net: Combining LSTM and U-net for sinogram synthesis in sparse-view SPECT reconstruction," *Math. Biosci. Eng.*, vol. 19, no. 4, pp. 4320–4340, 2022.
- [38] S. Hochreiter and J. Schmidhuber, "Long short-term memory," *Neural Comput.*, vol. 9, no. 8, pp. 1735–1780, 1997.
- [39] T. Okamoto, T. Ohnishi, and H. Haneishi, "Artifact reduction for sparse-view CT using deep learning with band patch," *IEEE Trans. Radiat. Plasma Med. Sci.*, vol. 6, no. 8, pp. 859–873, Nov. 2022.
- [40] J. Bai, X. Dai, Q. Wu, and L. Xie, "Limited-view CT reconstruction based on autoencoder-like generative adversarial networks with joint loss," in *Proc. IEEE Eng. Med. Biol. Soc.*, 2018, pp. 5570–5574.
- [41] R. Anirudh, H. Kim, J. J. Thiagarajan, K. A. Mohan, K. Champlay, and T. Bremer, "Lose the views: Limited angle CT reconstruction via implicit sinogram completion," in *Proc. IEEE Conf. Comput. Vis. Pattern Recognit.*, 2018, pp. 6343–6352.
- [42] H. S. Park, S. M. Lee, H. P. Kim, J. K. Seo, and Y. E. Chung, "CT sinogram-consistency learning for metal-induced beam hardening correction," *Med. Phys.*, vol. 45, no. 12, pp. 5376–5384, 2018.
- [43] G. Wang, D. L. Snyder, J. A. O'Sullivan, and M. W. Vannier, "Iterative deblurring for CT metal artifact reduction," *IEEE Trans. Med. Imag.*, vol. 15, no. 5, pp. 657–664, Oct. 1996.
- [44] G. Wang, T. Frei, and M. W. Vannier, "Fast iterative algorithm for metal artifact reduction in X-ray CT," *Acad. Radiol.*, vol. 7, no. 8, pp. 607–614, 2000.
- [45] A. Pimkin et al., "Multidomain CT metal artifacts reduction using partial convolution based inpainting," in *Proc. Int. Joint Conf. Neural Netw.*, 2020, pp. 1–6.
- [46] C. Peng et al., "An irregular metal trace inpainting network for X-ray CT metal artifact reduction," *Med. Phys.*, vol. 47, no. 9, pp. 4087–4100, 2020.
- [47] G. Liu, F. A. Reda, K. J. Shih, T.-C. Wang, A. Tao, and B. Catanzaro, "Image inpainting for irregular holes using partial convolutions," in *Proc. Eur. Conf. Comput. Vis.*, 2018, pp. 85–100.
- [48] Z. Li et al., "FD-MAR: Fourier dual-domain network for CT metal artifact reduction," 2022, *arXiv:2207.11678*.
- [49] H. Zhang et al., "Image prediction for limited-angle tomography via deep learning with convolutional neural network," 2016, *arXiv:1607.08707*.
- [50] Y. Huang et al., "Restoration of missing data in limited angle tomography based on Helgason–Ludwig consistency conditions," *Biomed. Phys. Eng. Exp.*, vol. 3, no. 3, 2017, Art. no. 35015.
- [51] Y. Huang, A. Preuhs, G. Lauritsch, M. Manhart, X. Huang, and A. Maier, "Data consistent artifact reduction for limited angle tomography with deep learning prior," in *Proc. Int. Workshop Mach. Learn. Med. Image. Reconstruct.*, 2019, pp. 101–112.
- [52] Y. Han, J. Gu, and J. C. Ye, "Deep learning interior tomography for region-of-interest reconstruction," 2017, *arXiv:1712.10248*.
- [53] Y. Han and J. C. Ye, "One network to solve all ROIs: Deep learning CT for any ROI using differentiated backprojection," *Med. Phys.*, vol. 46, no. 12, pp. e855–e872, 2019.
- [54] S. Xie et al., "Artifact removal using improved GoogLeNet for sparse-view CT reconstruction," *Sci. Rep.*, vol. 8, no. 1, pp. 1–9, 2018.
- [55] Z. Zhang, X. Liang, X. Dong, Y. Xie, and G. Cao, "A sparse-view CT reconstruction method based on combination of DenseNet and deconvolution," *IEEE Trans. Med. Imag.*, vol. 37, no. 6, pp. 1407–1417, Jun. 2018.
- [56] Y. Han and J. C. Ye, "Framing U-net via deep convolutional framelets: Application to sparse-view CT," *IEEE Trans. Med. Imag.*, vol. 37, no. 6, pp. 1418–1429, Jun. 2018.

- [57] J. C. Ye, Y. Han, and E. Cha, "Deep convolutional Framelets: A general deep learning framework for inverse problems," *SIAM J. Imag. Sci.*, vol. 11, no. 2, p. 51, 2017.
- [58] Y. Zhang and H. Yu, "Convolutional neural network based metal artifact reduction in X-ray computed tomography," *IEEE Trans. Med. Imag.*, vol. 37, no. 6, pp. 1370–1381, Jun. 2018.
- [59] L. Gjesteby et al., "A dual-stream deep convolutional network for reducing metal streak artifacts in CT images," *Phys. Med. Biol.*, vol. 64, no. 23, 2019, Art. no. 235003.
- [60] L. Yu, Z. Zhang, X. Li, and L. Xing, "Deep sinogram completion with image prior for metal artifact reduction in CT images," *IEEE Trans. Med. Imag.*, vol. 40, no. 1, pp. 228–238, Jan. 2021.
- [61] K. Liang, H. Yang, and Y. Xing, "Comparison of projection domain, image domain, and comprehensive deep learning for sparse-view X-ray CT image reconstruction," 2018, *arXiv:1804.04289*.
- [62] C. Sun, K. Deng, Y. Liu, and H. Yang, "A lightweight dual-domain attention framework for sparse-view CT reconstruction," 2022, *arXiv:2202.09609*.
- [63] N. Ma, X. Zhang, H.-T. Zheng, and J. Sun, "ShuffleNet v2: Practical guidelines for efficient CNN architecture design," in *Proc. Eur. Conf. Comput. Vis. (ECCV)*, 2018, pp. 116–131.
- [64] Y. Han, D. Wu, K. Kim, and Q. Li, "End-to-end deep learning for interior tomography with low-dose X-ray CT," *Phys. Med. Biol.*, vol. 67, no. 11, 2022, Art. no. 115001.
- [65] C. Chen, Y. Xing, L. Zhang, and Z. Chen, "Extraction-based deep learning reconstruction of interior tomography," 2022, *arXiv:2209.10350*.
- [66] J. H. Ketola, H. Heino, M. A. Juntunen, M. T. Nieminen, S. Siltanen, and S. I. Inkkinen, "Generative adversarial networks improve interior computed tomography angiography reconstruction," *Biomed. Phys. Eng. Exp.*, vol. 7, no. 6, 2021, Art. no. 65041.
- [67] Y. Lyu, W.-A. Lin, H. Liao, J. Lu, and S. K. Zhou, "Encoding metal mask projection for metal artifact reduction in computed tomography," in *Proc. Int. Conf. Med. Image Comput. Assist. Intervent.*, 2020, pp. 147–157.
- [68] T. Wang et al., "IDOL-Net: An interactive dual-domain parallel network for CT metal artifact reduction," *IEEE Trans. Radiat. Plasma Med. Sci.*, vol. 6, no. 8, pp. 874–885, Nov. 2022.
- [69] X. Gao et al., "Dual-domain attention-based deep network for sparse-view CT artifact reduction," 2022, *arXiv:2203.09169*.
- [70] D. Hu et al., "SPECIAL: Single-shot projection error correction integrated adversarial learning for limited-angle CT," *IEEE Trans. Comput. Imag.*, vol. 7, pp. 734–746, 2021.
- [71] C. Chen, Y. Xing, H. Gao, L. Zhang, and Z. Chen, "Sam's Net: A self-augmented multi-stage deep-learning network for end-to-end reconstruction of limited angle CT," *IEEE Trans. Med. Imag.*, vol. 41, no. 10, pp. 2912–2924, Oct. 2022.
- [72] T. Wang et al., "DAN-Net: Dual-domain adaptive-scaling non-local network for CT metal artifact reduction," *Phys. Med. Biol.*, vol. 66, no. 15, Jul. 2021, Art. no. 155009. [Online]. Available: <https://doi.org/10.1088/1361-6560/ac1156>
- [73] B. Zhu, J. Z. Liu, S. F. Cauley, B. R. Rosen, and M. S. Rosen, "Image reconstruction by domain-transform manifold learning," *Nature*, vol. 555, no. 7697, pp. 487–492, 2018.
- [74] L. Fu and B. De Man, "A hierarchical approach to deep learning and its application to tomographic reconstruction," in *Proc. 15th Int. Meeting Fully Three-Dimensional Image Reconstruct. Radiol. Nucl. Med.*, 2019, Art. no. 1107202.
- [75] Y. Li, K. Li, C. Zhang, J. Montoya, and G.-H. Chen, "Learning to reconstruct computed tomography images directly from sinogram data under a variety of data acquisition conditions," *IEEE Trans. Med. Imag.*, vol. 38, no. 10, pp. 2469–2481, Oct. 2019.
- [76] J. He, Y. Wang, and J. Ma, "Radon inversion via deep learning," *IEEE Trans. Med. Imag.*, vol. 39, no. 6, pp. 2076–2087, Jun. 2020.
- [77] V. Kandarpa, A. Bousse, D. Benoit, and D. Visvikis, "DUG-RECON: A framework for direct image reconstruction using convolutional generative networks," *IEEE Trans. Radiat. Plasma Med. Sci.*, vol. 5, no. 1, pp. 44–53, Jan. 2021.
- [78] V. Kandarpa, A. Perelli, A. Bousse, and D. Visvikis, "LRR-CED: Low-resolution reconstruction-aware convolutional encoder-decoder network for direct sparse-view CT image reconstruction," *Phys. Med. Biol.*, vol. 67, no. 15, Art. no. 155007, 2022.
- [79] B. Zhou, X. Lin, and B. Eck, "Limited angle tomography reconstruction: Synthetic reconstruction via unsupervised sinogram adaptation," in *Proc. Int. Conf. Inf Process. Med. Imag.*, 2019, pp. 141–152.
- [80] H. Liao, W.-A. Lin, S. K. Zhou, and J. Luo, "ADN: Artifact disentanglement network for unsupervised metal artifact reduction," *IEEE Trans. Med. Imag.*, vol. 39, no. 3, pp. 634–643, Mar. 2020.
- [81] Z. Shi, N. Wang, F. Kong, H. Cao, and Q. Cao, "A semi-supervised learning method of latent features based on convolutional neural networks for CT metal artifact reduction," *Med. Phys.*, vol. 49, no. 6, pp. 3845–3859, 2022.
- [82] C. Niu et al., "Low-dimensional manifold constrained disentanglement network for metal artifact reduction," *IEEE Trans. Radiat. Plasma Med. Sci.*, vol. 6, no. 6, pp. 656–666, Jul. 2022.
- [83] Y. Lyu, J. Fu, C. Peng, and S. K. Zhou, "U-DuDoNet: Unpaired dual-domain network for CT metal artifact reduction," in *Proc. Int. Conf. Med. Image Comput. Assist. Intervent.*, 2021, pp. 296–306.
- [84] H. Lan, L. Huang, L. Nie, and J. Luo, "Cross-domain unsupervised reconstruction with equivariance for photoacoustic computed tomography," 2023, *arXiv:2301.06681*.
- [85] J. Zhao, Z. Chen, L. Zhang, and X. Jin, "Unsupervised learnable sinogram inpainting network (SIN) for limited angle CT reconstruction," 2018, *arXiv:1811.03911*.
- [86] J. Lee, J. Gu, and J. C. Ye, "Unsupervised CT metal artifact learning using attention-guided β -CycleGAN," *IEEE Trans. Med. Imag.*, vol. 40, no. 12, pp. 3932–3944, Dec. 2021.
- [87] B. Zhao, J. Li, Q. Ren, and Y. Zhong, "Unsupervised reused convolutional network for metal artifact reduction," in *Proc. Int. Conf. Neural Inf. Process.*, 2020, pp. 589–596.
- [88] D. Ulyanov, A. Vedaldi, and V. Lempitsky, "Deep image prior," in *Proc. IEEE Conf. Comput. Vis. Pattern Recognit.*, 2018, pp. 9446–9454.
- [89] M. Wu, Y. Xu, Y. Xu, G. Wu, Q. Chen, and H. Lin, "Adaptively reweighting multi-loss untrained transformer for sparse-view cone-beam CT reconstruction," 2022, *arXiv:2203.12476*.
- [90] A. Dosovitskiy et al., "An image is worth 16x16 words: Transformers for image recognition at scale," in *Proc. Int. Conf. Learn. Represent.*, 2021, pp. 1–21. [Online]. Available: <https://openreview.net/forum?id=YicbFdNTTy>
- [91] I. Higgins et al., "Beta-VAE: Learning basic visual concepts with a constrained variational framework," in *Proc. Int. Conf. Learn. Represent.*, 2017, pp. 1–22. [Online]. Available: <https://openreview.net/forum?id=Sy2fzU9gI>
- [92] T. Wang, H. Yu, Z. Lu, Z. Zhang, J. Zhou, and Y. Zhang, "SemiMAR: Semi-supervised learning for CT metal artifact reduction," *IEEE J. Biomed. Health Inform.*, early access, Sep. 5, 2023, doi: [10.1109/JBHI.2023.3312292](https://doi.org/10.1109/JBHI.2023.3312292).
- [93] T. R. Moen et al., "Low-dose CT image and projection dataset," *Med. Phys.*, vol. 48, no. 2, pp. 902–911, 2021.
- [94] W. Wu, D. Hu, C. Niu, H. Yu, V. Vardhanabhuti, and G. Wang, "DRONE: Dual-domain residual-based optimization network for sparse-view CT reconstruction," *IEEE Trans. Med. Imag.*, vol. 40, no. 11, pp. 3002–3014, Nov. 2021.
- [95] K. Clark et al., "The cancer imaging archive (TCIA): Maintaining and operating a public information repository," *J. Digit. Imag.*, vol. 26, no. 6, pp. 1045–1057, Jul. 2013. [Online]. Available: <http://dx.doi.org/10.1007/s10278-013-9622-7>
- [96] M. Nauwynck et al., "Ring artifact reduction in sinogram space using deep learning," in *Proc. Int. Conf. Image Formation X-ray Computed Tomography*, Regensburg, Germany, 2020, pp. 1–4.
- [97] T. Fu et al., "Deep-learning-based ring artifact correction for tomographic reconstruction," *J. Synchrot. Radiat.*, vol. 30, no. 3, pp. 620–626, 2023.
- [98] K. Yan, X. Wang, L. Lu, and R. M. Summers, "DeepLesion: Automated mining of large-scale lesion annotations and universal lesion detection with deep learning," *J. Med. Imag.*, vol. 5, no. 3, 2018, Art. no. 36501.
- [99] B. Glocker, D. Zikic, E. Konukoglu, D. R. Haynor, and A. Criminisi, "Vertebrae localization in pathological spine CT via dense classification from sparse annotations," in *Proc. Int. Conf. Med. Image Comput. Assist. Intervent.*, 2013, pp. 262–270.
- [100] C. McCollough, "TU-FG-207A-04: Overview of the low dose CT grand challenge," *Med. Phys.*, vol. 43, pp. 3759–3760, Jun. 2016.
- [101] P. Liu et al., "Deep learning to segment pelvic bones: Large-scale CT datasets and baseline models," *Int. J. Comput. Assist. Radiol. Surg.*, vol. 16, pp. 749–756, Apr. 2021.

- [102] M. Ronchetti, "TorchRadon: Fast differentiable routines for computed tomography," 2020, *arXiv:2009.14788*.
- [103] D. Micieli, T. Minniti, and G. Gorini, "NeuTomPy toolbox, a python package for tomographic data processing and reconstruction," *SoftwareX*, vol. 9, pp. 260–264, Jan.–Jun. 2019.
- [104] D. Hu et al., "Hybrid-domain neural network processing for sparse-view CT reconstruction," *IEEE Trans. Radiat. Plasma Med. Sci.*, vol. 5, no. 1, pp. 88–98, Jan. 2021.
- [105] L. Yu, Z. Zhang, X. Li, H. Ren, W. Zhao, and L. Xing, "Metal artifact reduction in 2D CT images with self-supervised cross-domain learning," *Phys. Med. Biol.*, vol. 66, no. 17, 2021, hboxArt. no. 175003.
- [106] V. Antun, F. Renna, C. Poon, B. Adcock, and A. C. Hansen, "On instabilities of deep learning in image reconstruction and the potential costs of AI," *Proc. Nat. Acad. Sci.*, vol. 117, no. 48, pp. 30088–30095, 2020.
- [107] A. Krull, T.-O. Buchholz, and F. Jug, "Noise2void-learning denoising from single noisy images," in *Proc. IEEE Conf. Comput. Vis. Pattern Recognit.*, 2019, pp. 2129–2137.
- [108] J. Batson and L. Royer, "Noise2Self: Blind denoising by self-supervision," in *Proc. Int. Conf. Mach. Learn.*, vol. 97, Jun. 2019, pp. 524–533. [Online]. Available: <https://proceedings.mlr.press/v97/batson19a.html>
- [109] A. A. Hendriksen, D. M. Pelt, and K. J. Batenburg, "Noise2inverse: Self-supervised deep convolutional denoising for tomography," *IEEE Trans. Comput. Imag.*, vol. 6, pp. 1320–1335, 2020.
- [110] C. Niu et al., "Noise suppression with similarity-based self-supervised deep learning," *IEEE Trans. Med. Imag.*, vol. 42, no. 6, pp. 1590–1602, Jun. 2023.
- [111] W. Xia, W. Cong, and G. Wang, "Patch-based denoising diffusion probabilistic model for sparse-view CT reconstruction," 2022, *arXiv:2211.10388*.
- [112] W. Xia, C. Niu, W. Cong, and G. Wang, "Cube-based 3D denoising diffusion probabilistic model for cone beam computed tomography reconstruction with incomplete data," 2023, *arXiv:2303.12861*.
- [113] B. Guan et al., "Generative modeling in sinogram domain for sparse-view CT reconstruction," 2022, *arXiv:2211.13926*.
- [114] Y. Song, L. Shen, L. Xing, and S. Ermon, "Solving inverse problems in medical imaging with score-based generative models," 2021, *arXiv:2111.08005*.
- [115] M. Selim, J. Zhang, M. A. Brooks, G. Wang, and J. Chen, "DiffusionCT: Latent diffusion model for CT image standardization," 2023, *arXiv:2301.08815*.
- [116] A. Dosovitskiy et al., "An image is worth 16x16 words: Transformers for image recognition at scale," 2021, *arXiv:2010.11929*.